COMPDYN 2015
5th ECCOMAS Thematic Conference on
Computational Methods in Structural Dynamics and Earthquake Engineering
M. Papadrakakis, V. Papadopoulos, V. Plevris (eds.)
Crete Island, Greece, 25–27 May 2015

VERTICAL ACCELERATION DEMANDS ON NONSTRUCTURAL COMPONENTS IN BUILDINGS

L. Moschen[1], R. A. Medina[2], and C. Adam[1]

[1]Unit of Applied Mechanics, Department of Engineering Science, University of Innsbruck, Austria
Technikerstr. 13, 6020 Innsbruck, Austria
e-mail: {lukas.moschen,christoph.adam}@uibk.ac.at

[2]Department of Civil and Environmental Engineering, University of New Hampshire, U.S.A.
Kingsbury Hall Room W137, 33 Academic Way, 03824 Durham, NH, U.S.A.
e-mail: ricardo.a.medina@unh.edu

Keywords: Design Vertical Acceleration Response Spectrum, Vertical Ground Motion Selection, Perimeter Frames, Peak Vertical Acceleration Demands, Nonstructural Components.

Abstract. *This paper addresses the statistical evaluation of vertical peak floor acceleration (PFA_v) demands on elastic multistory buildings using recorded ground motions. Typical buildings are considered to be relatively flexible in the horizontal (lateral) direction and relatively rigid in the vertical (longitudinal) direction. The vast majority of studies conducted on the quantification of component acceleration demands have considered the flexibility of the nonstructural component (NSC) and its supporting structure primarily in the lateral direction. Studies on the evaluation of vertical component acceleration demands throughout a building are scarce and different opinions exist on the relevance of vertical accelerations in buildings. This paper focuses on the quantification of PFA_v, which implies that NSCs are assumed to be rigid in the vertical direction. Only rigid NSCs located close to columns of moment-resisting frames are considered. Thus, the influence of vertical floor vibrations and their dependence on the properties of the floor system is not addressed. The results demonstrate that the amplification of vertical ground acceleration demands throughout a building depends on the vertical stiffness of the load bearing structure, and hence, the common assumption of rigid-body responses in the vertical direction is highly questionable.*

1 INTRODUCTION

Many studies have been conducted during the last decades to assess seismic acceleration demands on nonstructural components (NSCs, also referred to secondary structures, building contents, mechanical and electrical equipment, architectural components) attached to elastic and inelastic buildings. Most research activities have focused on the horizontal acceleration components of ground motions. As a result, design engineers have relied upon simplified equations provided by building codes [1–3] to estimate the maximum horizontal acceleration demands on NSCs with much less attention been paid to maximum vertical acceleration demands.

Currently, a relatively small number of studies incorporates the effect of the vertical component of ground motions and its corresponding vertical floor motions. Generally, structural systems commonly used in buildings are considered to be relatively flexible in the lateral direction and relatively rigid in the vertical (longitudinal) direction. If columns were axially rigid, negligible amplification of the vertical component of the ground motion would occur for NSCs located at or near columns. On the other hand, for NSCs located at open-bays, i.e., at locations away from columns and relatively close to girders or in the middle of slabs, an amplification of the vertical floor acceleration with respect to ground has the potential to be significant. This is a result of resonance effects due to the out-of-plane flexibility of the girder/slab and the frequency content of the base excitation [4]. Therefore, vertical floor accelerations are highly dependent on the location of the component in a specific floor, the location of the component along the height of the building, and the characteristics and properties of the floor system.

For NSCs of various frequencies, a rigorous and comprehensive evaluation of their response must consider floor response spectra. This is particularly important given the myriad of periods (in this case horizontal vibration periods) associated with secondary structures such as electrical and mechanical equipment. These systems are generally classified as acceleration-sensitive because of their relatively large stiffness. In the United States of America, components are classified as either rigid or flexible based on their horizontal fundamental period, where NSCs with a period $T_s < 0.06\,\mathrm{s}$ are denoted as rigid [5]. Hence, flexible NSCs are susceptible to experiencing significant amplification of acceleration responses with respect to ground. In the specific case of vertical floor motions, and based on the study presented in [4], the flexibility of the girder/slab plays an important role.

Design forces for nonstructural components due to vertical base excitation are proposed in standards of the United States of America [1, 2]. In contrast, the European standard [3] does not provide explicit information on design vertical component accelerations or forces. In the United States of America, the recommended design component forces in the vertical direction $F_{p,v}$ are simply $50\,\%$ of the product of the design horizontal peak ground acceleration PGA_h times the seismic active mass in vertical direction:

$$F_{p,v} = \pm 0.20\, S_{DS} W_p = \pm 0.50\, PGA_h W_p \tag{1}$$

where S_{DS} is the design horizontal spectral acceleration in the short period region, and W_p is the operating mass of the component.

In contrast to the definition in [1], in this study the subscripts v and h are used in order to clearly define the difference between horizontal and vertical direction. However, this simplified estimation is questionable since the proposed equation for vertical component forces is not based on rigorous analyses or reliable experience data. One of the main problems is the lack of recorded vertical responses from buildings due to general unavailability of buildings instrumented with accelerometers able to record vertical motions. Thus, there is the need to quantify peak vertical floor acceleration demands (PFA_v) and their associated vertical floor response spectra.

2 GROUND MOTION RECORD SELECTION

Any ground motion record selection approach based on seismic hazard information necessitates the availability of vertical pseudo-spectral acceleration spectra ($S_{a,v}\left(T,\zeta\right)$). Unfortunately, probabilistic seismic hazard information is only available for the horizontal component of ground motions. Campbell and Bozorgnia [6, 7] developed a procedure to address this challenge without having to conduct a full-blown probabilistic seismic hazard analysis for the vertical component of ground motion. The first step involves converting the $\zeta = 5\,\%$ damped horizontal spectral acceleration at a period of $0.20\,\mathrm{s}$ $S_{a,h}\left(T = 0.20\,\mathrm{s},\zeta\right)$ to vertical spectral accelerations using vertical-to-horizontal (V/H) acceleration ratios for the site class BC boundary [8]. These ratios were estimated based on a study that involves near-source strong ground motions [6]. The second step entails the estimation of vertical spectral ordinates at all periods based on the vertical spectral ordinate at $T = 0.10\,\mathrm{s}$, modified for appropriate site conditions.

As part of the National Earthquake Hazards Reduction Program (NEHRP) in the U.S., a $\zeta = 5\,\%$ damped design vertical acceleration spectrum was proposed in [8]. The design vertical acceleration spectrum is based on modifications made to the procedure proposed by Campbell and Bozorgnia [7]. The primary modification involved estimating design vertical spectral accelerations from horizontal spectral acceleration values, which are available in seismic design maps [9]. These seismic design maps were obtained from hazard analysis using ground motion records that are part of the NGA ground motion database [10], which is the database used in this study to select ground motion records. A modified conversion factor is introduced in [8] to transform design horizontal to design vertical spectral accelerations for all soil conditions. In this process, estimates of design horizontal spectral accelerations are obtained from the $\mathrm{MCE_R}$ (risk-targeted Maximum Considered Earthquake) horizontal spectral acceleration at a period of $T = 0.20\,\mathrm{s}$ (S_S) [1]. These $\mathrm{MCE_R}$ values are provided in seismic design maps. Once this modified conversion is applied, limits are set on the design vertical spectral accelerations, and ordinates at periods other than $0.10\,\mathrm{s}$ are estimated based on relationships that are a function of the period in the vertical direction [8]. This transformation is possible primarily because for most soil conditions, as well as for magnitudes ($M_W > 6.5$) and focal distances ($r_{jb} < 60\,\mathrm{km}$) (Joyner-Boore dinstance) of interest for engineered structures, the (V/H) ratio $S_{a,v}\left(T = 0.10\,\mathrm{s},\zeta\right)/S_{a,h}\left(T = 0.20\,\mathrm{s},\zeta\right)$ is about 0.80 [8].

The approach described above leads to the vertical response spectrum in [8] (from here on referred to in this paper as NEHRP-spectrum). Figure 1 shows the normalized vertical spectral ordinate over the vertical frequency in Hz, $f_v = 1/T_v$. Spectral ordinates are normalized by the acceleration due to gravity g and $C_V S_{DS}$, where C_V can be obtained from Table 1 and S_{DS} is the design horizontal spectral acceleration at short periods according to [1, 8]. The normalized NEHRP-spectrum can be constructed by evaluation of:

$$\frac{S_{a,v}(f_v,\zeta)}{g\,C_V S_{DS}} = \begin{cases} 0.3 & \text{if } f_v \geq 40\,\mathrm{Hz} \\ 2.0\left(1/f_v - 1/40\right) + 0.3 & \text{if } 20\,\mathrm{Hz} \leq f_v \leq 40\,\mathrm{Hz} \\ 0.8 & \text{if } 20/3\,\mathrm{Hz} \leq f_v \leq 20\,\mathrm{Hz} \\ 0.8\left(20/3\,f_v\right)^{3/4} & \text{if } 0\,\mathrm{Hz} \leq f_v \leq 20/3\,\mathrm{Hz} \end{cases} \tag{2}$$

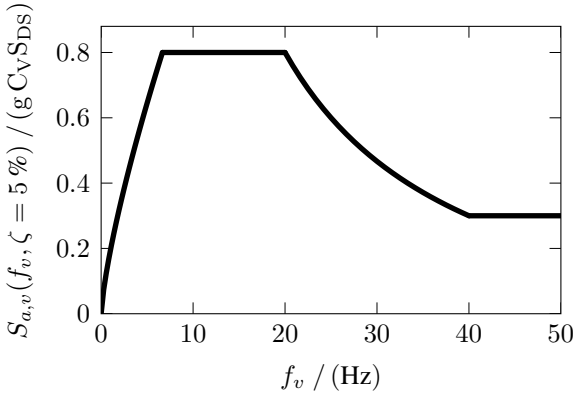

Figure 1: Normalized vertical design response spectrum (NEHRP-spectrum).

S_S	C_V NEHRP Site Class		
	A, B	C	D, E, F
≥ 2.00	0.90	1.30	1.50
1.00	0.90	1.10	1.30
0.60	0.90	1.00	1.10
0.30	0.80	0.80	0.90
≤ 0.20	0.70	0.70	0.70

Table 1: Conversation factor C_V for different site classifications.

2.1 Selection of ground motions for compatibility with the NEHRP-spectrum

Currently, a consensus on how to select ground motions for response history analysis (RHA) is nonexistent. However, an approach that is widely accepted and used in the earthquake engineering community is the use of base accelerations whose spectral ordinates over a desired frequency range are consistent with a target spectrum that is representative of the site. In general, this target spectrum can be obtained from either seismic hazard analysis (e.g., a design response spectrum) or a scenario analysis (e.g., from a ground motion prediction equation, GMPE). A more comprehensive discussion regarding ground motion selection methods as well as their pros and cons can be found in [11].

The ground motion record selection in this paper is based on the NEHRP-spectrum, more specifically, on its spectral shape. Equation (2) shows that the regions of constant acceleration are independent of site conditions. In other words, the corner frequencies are constant (in contrast to those present in NEHRP design horizontal spectra). Therefore, this property of the vertical NEHRP-spectrum facilitates in part the selection of ground motion records from the NGA (PEER) ground motion database [12] based on how consistent the central value and the dispersions of the chosen record set is with the spectral shape of the NEHRP-spectrum. The proposed ground motion record selection method explicitly accounts for the record-to-record variability in the estimation of seismic demands, and hence, provides the means to evaluate seismic demands statistically.

2.2 Spectrum-compatible record sets

In order to evaluate seismic demands statistically, a set of records is required to account for the record-to-record variability. Finding spectrum-compatible ground motion record sets is a computational expensive procedure. Thus, the 3179 earthquake recordings provided by the NGA (PEER) ground motion database were evaluated and a subset of recordings pre-selected based on the following characteristics:

- Moment magnitude: $M_W \geq 5.50$.
- NEHRP Site Classification D (stiff soil, shear wave velocity: $180\,\text{m/s} \leq v_{s30} \leq 360\,\text{m/s}$).
- Fault mechanism (FM): strike-slip (SS), reverse (RV), reverse-oblique (RVO).
- Distance (as defined by Joyner and Boore [13]): $0\,\text{km} \leq r_{jb} \leq 30\,\text{km}$.

A comprehensive overview of the characterization of ground motions (magnitude, fault mechanism, source to site distance, etc.) can be found in [14].

In this paper, the motivation is to find a set of records with the same scale factor α applied to each record according to the following criteria:

- The median spectral acceleration for the set $\widetilde{S}_{a,v}(f_v, \zeta, \alpha)$ should match the normalized NEHRP-spectrum over the frequency range of interest.
- The dispersion, which is measured as the standard deviation of the natural logarithm of the values for a given frequency, $\sigma_{S_{a,v}(f_v,\zeta,\alpha)}$ should be equal to a predefined target dispersion $\sigma_t(f_v) = \sigma_t$.

These two targets constitute two different spectrum-matching requirements. This leads to two coupled objective functions that can be minimized using genetic algorithms implemented in Matlab [15] for multicomponent objective functions:

$$\left.\begin{aligned} F_1(\alpha) &= \left\| S_{a,v}(f_v,\zeta) - \widetilde{S}_{a,v}(f_v,\zeta,\alpha) \right\| \\ F_2(\alpha) &= \left\| \mathrm{e}^{\sigma_t} S_{a,v}(f_v,\zeta) - S_{84,a,v}(f_v,\zeta,\alpha) \right\| \end{aligned}\right\} \longrightarrow \min \tag{3}$$

In order to generate a record set independent of site conditions, the product of the conversion factor and the spectral acceleration at short periods was set to $C_V S_{DS} = 1.00\,\text{g}$ for the optimization procedure. Additionally, spectral accelerations for a given frequency are assumed to be log-normally distributed, which is typical for response quantities in earthquake engineering [16]. Therefore, 84th percentile values $S_{84,a,v}(f_v, \zeta, \alpha)$ can be estimated by the product of the parameter e^{σ_t} and the median spectral acceleration. The implementation of this approach for ground motion selection can be interpreted as semi-probabilistic since the choice of σ_t biases the record selection. However, a variation of the target dispersion of $\sigma_t = 0.4\,\text{g}$, $0.6\,\text{g}$, $0.8\,\text{g}$ and $1.0\,\text{g}$ is used to quantify this influence. This range of values is reasonable and in agreement with the range of dispersions depicted in the spectra of [17].

The solutions of the multi-objective optimization can be graphically interpreted as a Pareto-optimal solution [18], sometimes referred to as Pareto frontier. Possible realizations (i.e., spectrum matching record sets) are shown in Figures 3 to 6. Figures 3a to 6a show the spectra of individual records, their statistical measures, and the NEHRP-spectrum. Figures 3b to 6b show the distribution of the records as a function of magnitude-distance ($M_W - r_{jb}$) coordinates.

No.	recs	σ_t	α
1	55	0.40	1.98
2	62	0.60	1.89
3	91	0.80	2.10
4	82	1.00	2.55

Table 2: Basic characteristics of ground motion record sets compatible with the normalized NEHRP-spectrum.

Table 2 lists the basic properties of each record set; the total number of records in each set is given in the second column.

A qualitative evaluation of the median spectrum of each ground motion set shows that each median spectrum is an adequate approximation of the target spectrum in the region $0\,\text{Hz} \leq f_v \leq {}^{20}/_{3}\,\text{Hz}$ (Figures 3a to 6a). The quality of the approximation in the region around the corner frequency $f_v = 20\,\text{Hz}$ increases with increasing number of records (not with increasing dispersion as discussed later). Furthermore, the median spectrum of each record set fits optimally the NEHRP-spectrum at the frequency of $f_v \approx 27\,\text{Hz}$ and each record set over predicts the target spectrum in the high frequency region.

The distribution of ground motions with respect to magnitude and distance for each record set is shown in Figures 3b to 6b. It is evident that most of the ground motion records belong to earthquakes with moment magnitudes between $6.0 \leq M_W \leq 6.7$, as shown in Table 3.

In order to define an optimal record set out of the four sets presented in Table 2, an understanding of the influence of the number of records and the target dispersion is required. Therefore, the relation between number of records and target dispersion is depicted in Figure 2, where the markers show the data listed in Table 2 and the solid line is a smooth interpolation polynomial.

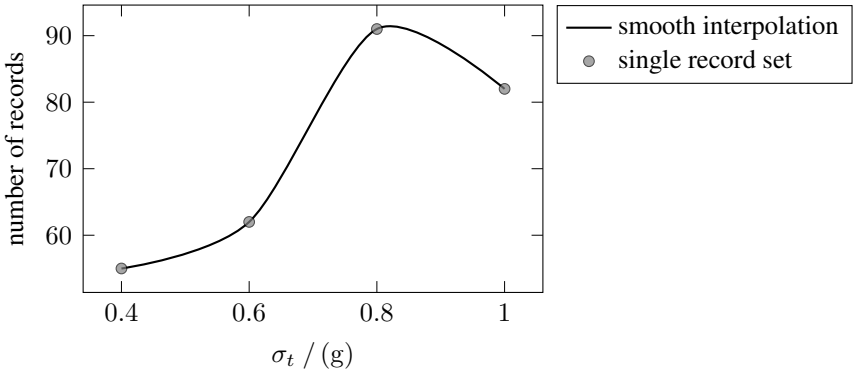

Figure 2: Relation between target dispersion σ_t and number of records (graphical interpretation of Table 2) and its smooth interpolation.

A larger number of records provides a closer and smoother approximation of the median to the NEHRP-spectrum. Moreover, when the target dispersion σ_t approaches zero, the spectrum of each ground motion record should closely match the target spectrum. This condition is only a theoretical consideration since each record has a different spectral shape. The probability density function (PDF) for this theoretical case degenerates from a log-normal distribution to the Dirac delta function. The conclusion is that competing objectives are present and, in general, increasing the number of records is required to obtain larger target dispersion values.

An optimal solution for the proposed record sets used in this paper can be obtained from Table 2 and from the graphical interpretation shown in Figure 2. Record set number three ($\sigma_t = 0.80$ g) consists of the maximum number of records. Comparison of the median spectrum between Figures 5a and 6a as well as a qualitative evaluation of the relative error in Figure 7 leads to a different conclusion than described before - record set number four shows fewer records than set number three but a median spectrum with a better compatibility with the NEHRP-spectrum. It can then be expected that a record set with a target dispersion of $0.80\,\text{g} \leq \sigma_t \leq 1.00\,\text{g}$ should lead to an optimal solution, i.e., a reasonable compromise between number of records, dispersion, and medium spectrum compatibility. Figure 2 shows that, based on the discrete values of dispersion used in this study, the peak value is very close to $\sigma_t = 0.80\,\text{g}$, thus the median of record set number three is selected as the optimal fit to the NEHRP-spectrum. From here on, in this paper, this record set is referred to as the VGM record set. The basic characteristics of the single ground motion records constituting the VGM record set are listed in Table 3.

A practical tool for selection of spectrum compatible record sets is currently under development of this research group and will be published to the community in the near future.

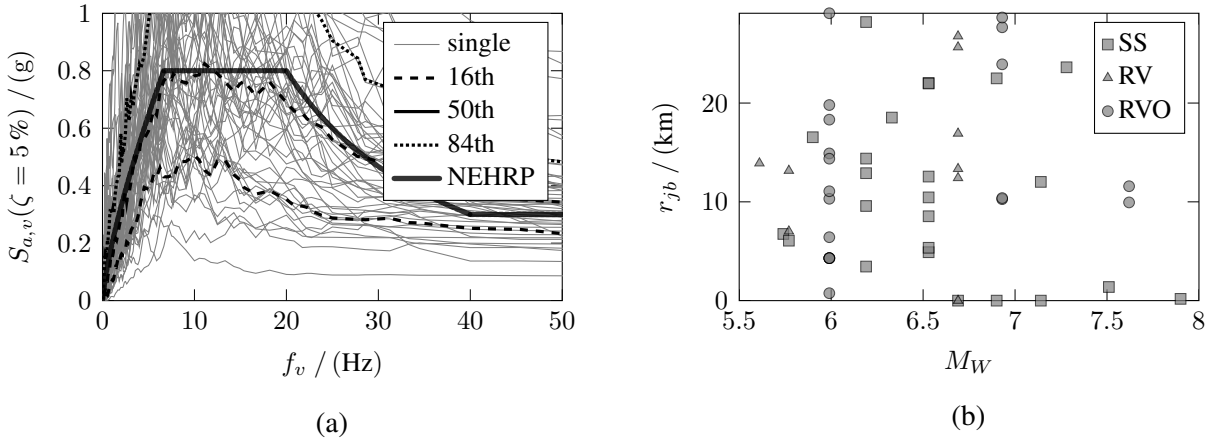

Figure 3: (a) Spectra of ground motion record sets and (b) distribution of records compatible with the normalized NEHRP-spectrum for a given target dispersion $\sigma_t = 0.40\,\text{g}$.

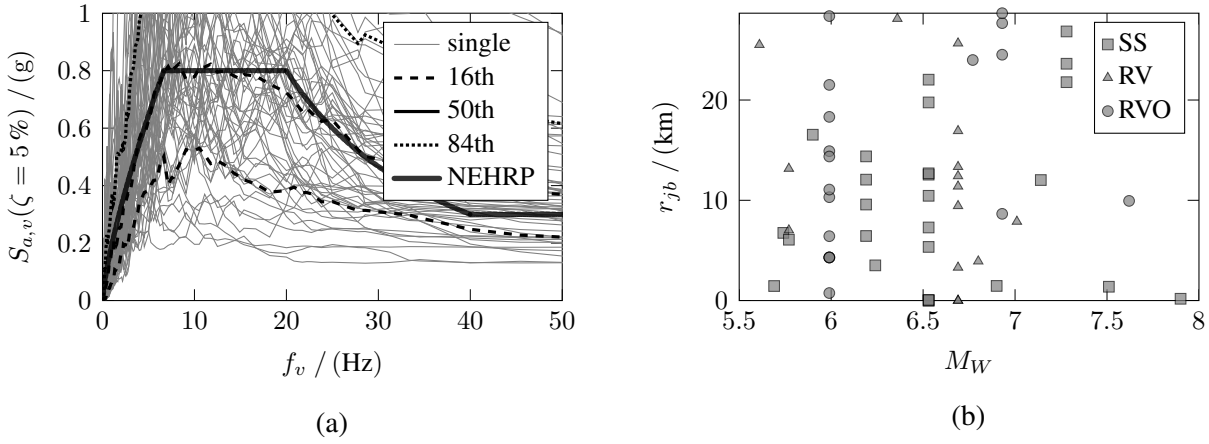

Figure 4: (a) Spectra of ground motion record sets and (b) distribution of records compatible with the normalized NEHRP-spectrum for a given target dispersion $\sigma_t = 0.60\,\text{g}$.

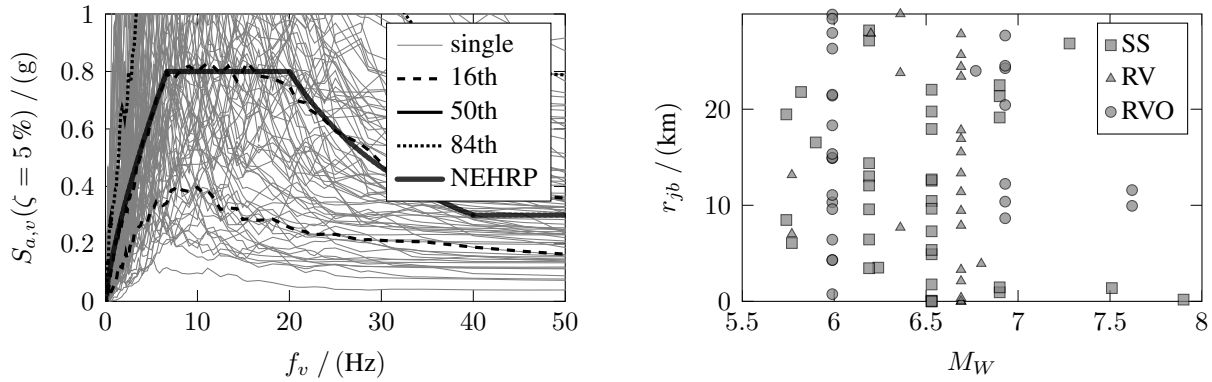

(a) (b)

Figure 5: (a) Spectra of ground motion record sets and (b) distribution of records compatible with the normalized NEHRP-spectrum for a given target dispersion $\sigma_t = 0.80$ g.

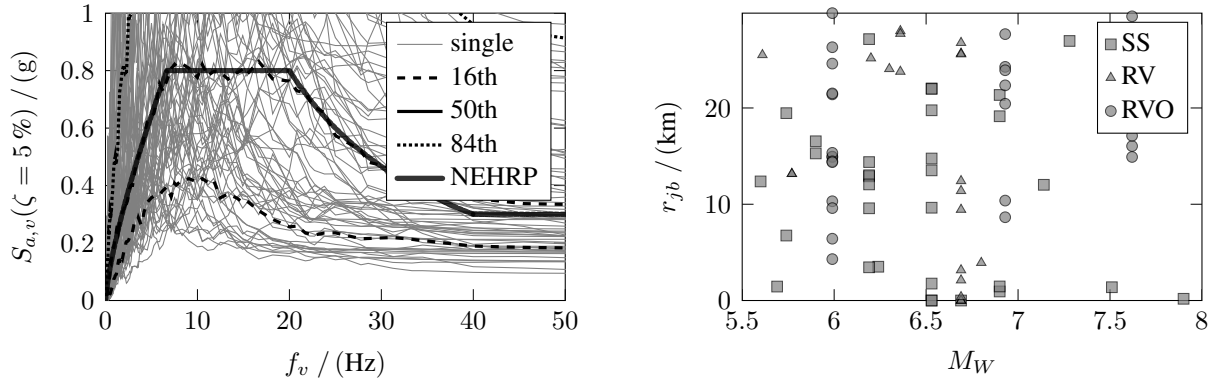

(a) (b)

Figure 6: (a) Spectra of ground motion record sets and (b) distribution of records compatible with the normalized NEHRP-spectrum for a given target dispersion $\sigma_t = 1.00$ g.

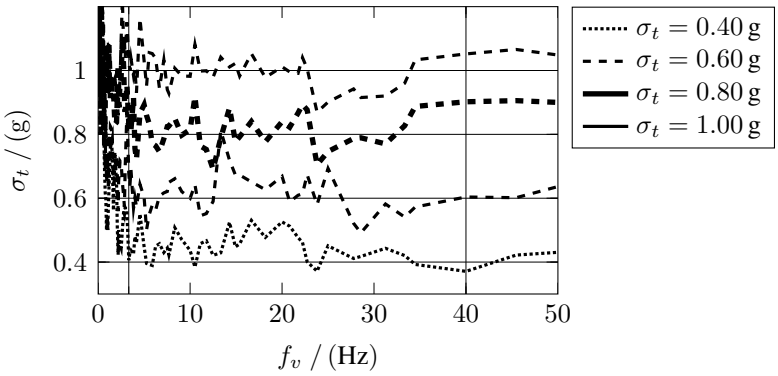

Figure 7: Variation with frequency of the dispersion of ground motion record sets compatible with the normalized NEHRP-spectrum for a given target dispersion.

No.	Earthquake Name	Station Name	Year	M_W	FM	r_{jb}/(km)
1	Parkfield	Cholame - Shandon Array 5	1966	6.19	SS	9.58
2	Managua, Nicaragua-01	Managua, ESSO	1972	6.24	SS	3.51
3	Gazli, USSR	Karakyr	1976	6.80	RV	3.92
4	Coyote Lake	Gilroy Array 2	1979	5.74	SS	8.47
5	Coyote Lake	San Juan Bautista, 24 Polk St	1979	5.74	SS	19.46
6	Imperial Valley-06	Aeropuerto Mexicali	1979	6.53	SS	0.00
7	Imperial Valley-06	Calexico Fire Station	1979	6.53	SS	10.45
8	Imperial Valley-06	Chihuahua	1979	6.53	SS	7.29
9	Imperial Valley-06	Delta	1979	6.53	SS	22.03
10	Imperial Valley-06	El Centro - Meloland Geot. Array	1979	6.53	SS	0.07
11	Imperial Valley-06	El Centro Array 1	1979	6.53	SS	19.76
12	Imperial Valley-06	El Centro Array 11	1979	6.53	SS	12.56
13	Imperial Valley-06	El Centro Array 12	1979	6.53	SS	17.94
14	Imperial Valley-06	El Centro Array 4	1979	6.53	SS	4.90
15	Imperial Valley-06	El Centro Array 5	1979	6.53	SS	1.76
16	Imperial Valley-06	El Centro Array 6	1979	6.53	SS	0.00
17	Imperial Valley-06	Holtville Post Office	1979	6.53	SS	5.35
18	Imperial Valley-06	Parachute Test Site	1979	6.53	SS	12.69
19	Imperial Valley-06	SAHOP Casa Flores	1979	6.53	SS	9.64
20	Westmorland	Parachute Test Site	1981	5.90	SS	16.54
21	Coalinga-01	Cantua Creek School	1983	6.36	RV	23.78
22	Coalinga-01	Parkfield - Fault Zone 7	1983	6.36	RV	29.91
23	Coalinga-01	Pleasant Valley P.P. - yard	1983	6.36	RV	7.69
24	Coalinga-05	Coalinga-14th Elm (Old CHP)	1983	5.77	RV	7.02
25	Coalinga-05	Pleasant Valley P.P. - yard	1983	5.77	RV	13.16
26	Morgan Hill	Gilroy Array 3	1984	6.19	SS	13.01
27	Morgan Hill	Gilroy Array 7	1984	6.19	SS	12.06
28	Morgan Hill	Halls Valley	1984	6.19	SS	3.45
29	Morgan Hill	San Juan Bautista, 24 Polk St	1984	6.19	SS	27.15
30	Bishop (Rnd Val)	McGee Creek - Surface	1984	5.82	SS	21.79
31	Chalfant Valley-01	Zack Brothers Ranch	1986	5.77	SS	6.07
32	Chalfant Valley-02	Bishop - LADWP South St	1986	6.19	SS	14.38
33	Chalfant Valley-02	McGee Creek - Surface	1986	6.19	SS	28.20
34	Chalfant Valley-02	Zack Brothers Ranch	1986	6.19	SS	6.44
35	Whittier Narrows-01	Bell Gardens - Jaboneria	1987	5.99	RVO	10.31
36	Whittier Narrows-01	Carson - Catskill Ave	1987	5.99	RVO	29.85
37	Whittier Narrows-01	Compton - Castlegate St	1987	5.99	RVO	18.32
38	Whittier Narrows-01	Downey - Birchdale	1987	5.99	RVO	14.90
39	Whittier Narrows-01	Downey - Co Maint Bldg	1987	5.99	RVO	14.95
40	Whittier Narrows-01	El Monte - Fairview Av	1987	5.99	RVO	0.75
41	Whittier Narrows-01	Hacienda Heights - Colima	1987	5.99	RVO	9.60
42	Whittier Narrows-01	Inglewood - Union Oil	1987	5.99	RVO	21.41
43	Whittier Narrows-01	LA - Baldwin Hills	1987	5.99	RVO	21.51
44	Whittier Narrows-01	LA - Fletcher Dr	1987	5.99	RVO	11.07
45	Whittier Narrows-01	LA - N Faring Rd	1987	5.99	RVO	27.94
46	Whittier Narrows-01	LA - N Westmoreland	1987	5.99	RVO	15.34
47	Whittier Narrows-01	Lawndale - Osage Ave	1987	5.99	RVO	26.31

Continued on next page

No.	Earthquake Name	Station Name	Year	M_W	FM	r_{jb}/(km)
48	Whittier Narrows-01	Pasadena - Brown Gym	1987	5.99	RVO	4.30
49	Whittier Narrows-01	Pasadena - CIT Calif Blvd	1987	5.99	RVO	4.30
50	Whittier Narrows-01	Playa Del Rey - Saran	1987	5.99	RVO	29.42
51	Whittier Narrows-01	West Covina - S Orange Ave	1987	5.99	RVO	6.42
52	Spitak, Armenia	Gukasian	1988	6.77	RVO	23.99
53	Loma Prieta	Agnews State Hospital	1989	6.93	RVO	24.27
54	Loma Prieta	Capitola	1989	6.93	RVO	8.65
55	Loma Prieta	Coyote Lake Dam (Downst)	1989	6.93	RVO	20.44
56	Loma Prieta	Gilroy Array 2	1989	6.93	RVO	10.38
57	Loma Prieta	Gilroy Array 3	1989	6.93	RVO	12.23
58	Loma Prieta	Hollister - South Pine	1989	6.93	RVO	27.67
59	Loma Prieta	Hollister Differential Array	1989	6.93	RVO	24.52
60	Landers	North Palm Springs	1992	7.28	SS	26.84
61	Northridge-01	Arleta - Nordhoff Fire Sta	1994	6.69	RV	3.30
62	Northridge-01	Beverly Hills - 14145 Mulhol	1994	6.69	RV	9.44
63	Northridge-01	Canoga Park - Topanga Can	1994	6.69	RV	0.00
64	Northridge-01	Canyon Country - W Lost Cany	1994	6.69	RV	11.39
65	Northridge-01	Hollywood - Willoughby Ave	1994	6.69	RV	17.82
66	Northridge-01	LA - Century City CC North	1994	6.69	RV	15.53
67	Northridge-01	LA - Fletcher Dr	1994	6.69	RV	25.66
68	Northridge-01	LA - N Westmoreland	1994	6.69	RV	23.40
69	Northridge-01	LA - Pico Sentous	1994	6.69	RV	27.82
70	Northridge-01	Moorpark - Fire Sta	1994	6.69	RV	16.92
71	Northridge-01	N Hollywood - Coldwater Can	1994	6.69	RV	7.89
72	Northridge-01	Newhall - W Pico Canyon Rd.	1994	6.69	RV	2.11
73	Northridge-01	Pacific Palisades - Sunset	1994	6.69	RV	13.34
74	Northridge-01	Playa Del Rey - Saran	1994	6.69	RV	24.42
75	Northridge-01	Rinaldi Receiving Sta	1994	6.69	RV	0.00
76	Northridge-01	Sylmar - Converter Sta	1994	6.69	RV	0.00
77	Northridge-01	Tarzana - Cedar Hill A	1994	6.69	RV	0.37
78	Kobe, Japan	KJMA	1995	6.90	SS	0.94
79	Kobe, Japan	Kakogawa	1995	6.90	SS	22.50
80	Kobe, Japan	OSAJ	1995	6.90	SS	21.35
81	Kobe, Japan	Shin-Osaka	1995	6.90	SS	19.14
82	Kobe, Japan	Takatori	1995	6.90	SS	1.46
83	Kocaeli, Turkey	Yarimca	1999	7.51	SS	1.38
84	Chi-Chi, Taiwan	CHY025	1999	7.62	RVO	19.07
85	Chi-Chi, Taiwan	CHY101	1999	7.62	RVO	9.94
86	Chi-Chi, Taiwan	CHY104	1999	7.62	RVO	18.02
87	Chi-Chi, Taiwan	TCU038	1999	7.62	RVO	25.42
88	Chi-Chi, Taiwan	TCU110	1999	7.62	RVO	11.58
89	Chi-Chi, Taiwan	TCU112	1999	7.62	RVO	27.48
90	Denali, Alaska	TAPS Pump Station 10	2002	7.90	SS	0.18
91	Chi-Chi, Taiwan-03	CHY025	1999	6.20	RV	27.88

Table 3: Basic characteristics of ground motion records constituting the VGM record set ($\sigma_t = 0.80\,\mathrm{g}$, $\alpha = 2.10$) compatible with the normalized NEHRP-spectrum.

3 GENERIC STICK MODELS

The generic stick models used throughout this paper are developed on the basis of an evaluation of modal properties of the steel frames from the SAC steel project [19] and the ATC-76-1 project [20]. In a pilot study, conducted by this research group [21], the modal properties of the perimeter frames from the aforementioned projects were evaluated. Results demonstrated that linear first-mode shapes are reasonable approximations to the fundamental mode shapes in the lateral and longitudinal direction of these steel frames. Additionally, an analytical expression in terms of a two term power series is used to quantify the relation between the fundamental periods in both lateral, T_{1h}, and longitudinal, T_{1v}, directions, as a function of the total number of stories, N, of the structure:

$$T_{1h} = 0.720N^{0.63} - 0.401 \tag{4}$$

$$T_{1v} = -3.602N^{-0.02} + 3.621 \tag{5}$$

Figure 8 shows a graphical representation of Equations (4) and (5). The squared markers in the scatter highlight the empirical data observed from structural models of the SAC steel project [19], and the circled scatter marks the data from the ATC-76-1 project [20]. Equations (4) and (5) and linear first-mode shapes in the lateral and longitudinal direction are the basis to develop generic stick models as shown below for an interior column of a perimeter frame.

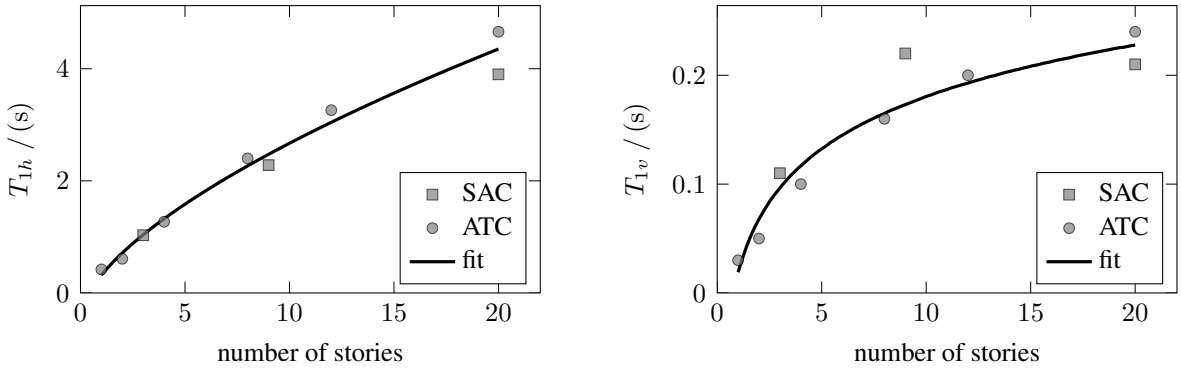

(a) (b)

Figure 8: Relation between (a) the fundamental period T_{1h} respectively (b) the fundamental period T_{1v} and the number of stories for the SAC steel project and the ATC-76-1 project.

Typical perimeter frames consist of two exterior columns and, if required, interior columns to transfer the effects of equivalent lateral forces from the structure to the foundation. Figure 9a shows schematically a six-story, two-bay generic frame. Lumped masses are depicted as gray circles. The degrees of freedom with respect to the ground $(x_g(t), z_g(t))$ are denoted as $x_i(t)$ in the lateral direction and as $z_i(t)$ in the vertical direction, where i is the floor number. In this context, a generic stick model represents an isolated column line of a frame as shown for the 6-story generic frame in Figure 9b for an interior column. In this paper the development of the generic stick model of interior columns is illustrated. The story and the floor numbering as well as the enumeration of the seismic mass are defined in Figure 9b. Figure 9c shows the generic stick model of the interior column consisting of columns, rotational springs $c_{\theta i}$ (representing the flexural stiffness of the frame) and vertical springs c_{ui} (representing the shear stiffness of the girders and the axial stiffness of the exterior columns). An additional rotational spring at the

base $c_{\theta 0}$ is required to make sure that the fundamental mode in the lateral direction is a straight line over the structure's height and to obtain a uniform distribution of the moments of inertia over the height [22].

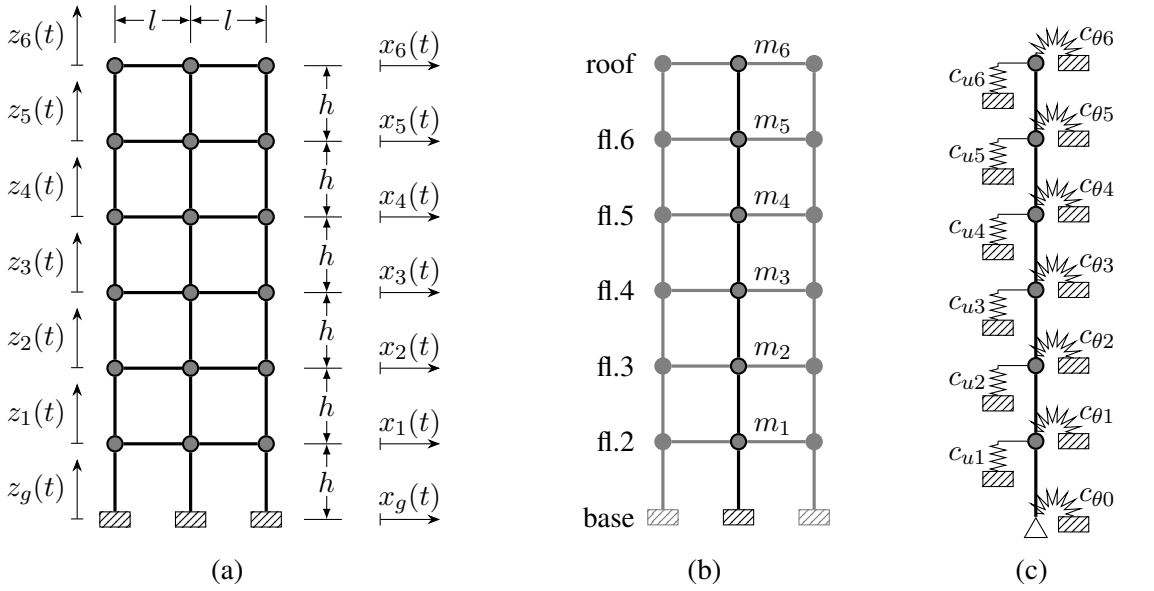

Figure 9: Development of generic stick models for interior columns based on a two-bay generic frame. (a) Complete generic frame, (b) isolated interior column with floor / story / mass numbering and (c) generic stick model including equivalent springs.

Furthermore, the assumptions outlined below are required for the development of models with appropriate flexibility in the vertical and horizontal directions:

- PΔ effects are not included. In other words, modal quantities are based on first-order analyses. Thus, the global stiffness matrix $\mathbf{K}$ does not include the geometric stiffness.
- Lumped masses as shown in Figure 9 are used. When modeling the structure with a generic stick, the mass matrix $\mathbf{M}$ is a diagonal matrix for the lateral as well as the vertical degrees of freedom.
- The story height h is the same for each story and the bay width is l for each one of them (see Figure 9).
- Since SAC and the ATC-76-1 frames are steel frames, Young's modulus of $E = 2 \cdot 10^{11}$ N/m^2 is used.
- Column splices are located at column mid-heights (except the columns of the first story, the splices of those members are located at mid height of the second story). Therefore, column cross sectional properties A_i and I_i between story mid-heights are constant. Furthermore, at each beam-column (BC) connection, column and girder member sizes are assumed to be the same as shown in Figure 10b for the ith floor.

3.1 Structural parameters in the lateral direction

In this study, it is assumed that the first mode dominates the structural response and the fundamental mode shape in the lateral direction is linear over the structure's height. The

deflected shape of the frame under lateral loading assumes points of inflection POIs at column mid-heights and beam mid-spans (Figure 10a). This assumption allows the use of the free-body diagram presented in Figure 10b by constraining the substructure using pinned supports at the POIs.

At each floor level, the same seismic masses $m_{ih}^{(l)}$, $m_{ih}^{(m)}$ and $m_{ih}^{(r)}$ are used at the left, mid, and right of the BC connection as shown in Figure 10b. Thus, the total seismic mass in the horizontal direction acting at each floor level of the perimeter frame equals:

$$m_h^{(story)} = m_{ih}^{(l)} + m_{ih}^{(m)} + m_{ih}^{(r)} \tag{6}$$

For this generic stick model only the mass associated with the interior column is required, therefore, $m_h = m_{ih}^{(m)}$, which implies that floor masses are constant with a value equal to that of the diagonal elements of the mass matrix $\mathbf{M}_h$ (note, the labels of the masses in Figure 9b don't have a subscript h to keep the figure independent from the lateral / vertical direction). The seismic mass can be determined from the dead load of the structure including the weight of cladding.

Equivalent lateral stiffness for the generic stick models can be obtained by imposing the deflected shape shown in Figure 10b to the various substructures along the height of the frame. Both exterior columns are the same. In particular, each BC connection consists of a half column of the lower story, a half column of the upper story, and a half girder. In contrast, the BC connection at the interior column is stiffer since two half girders frame into it.

The stiffness of an isolated BC connection can be expressed in terms of the relative lateral deformation u of the bottom and top column nodes in the free-body diagram of Figure 10b for a unit shear load. Thus, the individual contribution of the half columns below and above the girder to the total horizontal deflection is given by:

$$u^{(col)} = \frac{\left(h/2\right)^3}{3EI_i} \tag{7}$$

The deflection given by Equation (7) is equivalent to the deformation at the tip of a cantilever column of length $h/2$ that frames into a rigid girder when a unit shear load is applied. Now, if the girder is flexible and the column is considered to be rigid in flexure, then, the relative lateral deformation between the bottom and top column nodes in the free-body diagram of Figure 10b for a unit shear load is given by:

$$u^{(gir,int)} = 2\frac{l/2\left(h/2\right)^2}{3EI_i} \tag{8}$$

$$u^{(gir,ext)} = 4\frac{l/2\left(h/2\right)^2}{3EI_i} \tag{9}$$

The total substructure flexibility caused by the flexibility of the columns and the girder(s) is given by:

$$u^{(int)} = 2u^{(col)} + u^{(gir,int)} \tag{10}$$

$$u^{(ext)} = 2u^{(col)} + u^{(gir,ext)} \tag{11}$$

The equivalent lateral stiffness for each column line of the substructure of Figure 10b is then the

inverse of the flexibility given by Equations (10) and (11) and it is equal to:

$$c^{(int)} = \frac{1}{u^{(int)}} \tag{12}$$

$$c^{(ext)} = \frac{1}{u^{(ext)}} \tag{13}$$

Then, the total lateral story stiffness yields:

$$c^{(story)} = 2c^{(ext)} + c^{(int)} \tag{14}$$

Since the story shear force is directly proportional to the story mass (if damping is neglected), the seismic mass on the exterior columns and the interior column is proportional to the ratio between the individual joint stiffnesses and the total lateral stiffness for the substructure:

$$m_{ih}^{(m)} = \frac{c^{(int)}}{c^{(story)}} m_h^{(story)} = \frac{5}{11} m_h^{(story)} \tag{15}$$

$$m_{ih}^{(l)} = m_{ih}^{(r)} = \frac{c^{(ext)}}{c^{(story)}} m_h^{(story)} = \frac{3}{11} m_h^{(story)} \tag{16}$$

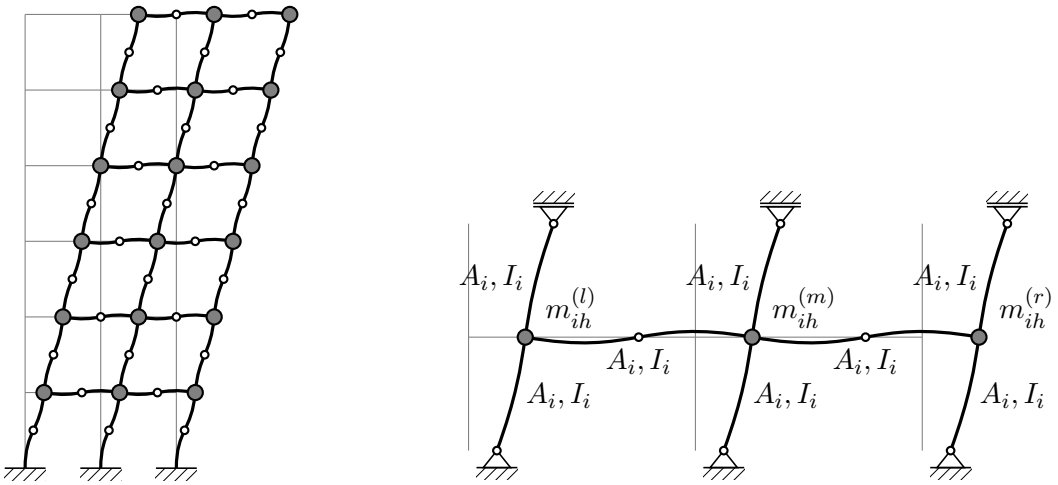

(a) (b)

Figure 10: Generic frame vibrating in its lateral linear fundamental mode. (a) Complete generic frame and (b) isolated substructure.

For vibration in the lateral direction the beam members are assumed to be axially rigid. The equivalent stiffness $c_{\theta i}$ of the rotational spring that represents the girders at the ith floor level (see Figure 10b) can be obtained by evaluation of:

$$c_{\theta i} = 2\frac{3EI_i}{l/2} = \frac{12EI_i}{l} \tag{17}$$

In order to obtain a uniform distribution of the moments of inertia over the structure's height a rotational spring is added at the base, which *simulates* beams framed at the bottom of the first story column:

$$c_{\theta 0} = 2\frac{3EI_1}{l/2} = \frac{12EI_1}{l} \tag{18}$$

Assembling the global mass- and stiffness matrix leads to the eigenvalue problem formulated in terms of the first eigenvalue and the corresponding linear mode shape:

$$(\mathbf{M}_h - \lambda_{1h}\mathbf{K}_h)\,\boldsymbol{\phi}_1 = \mathbf{0} \tag{19}$$

where the first eigenvalue λ_{1h} is the inversion of the square of the fundamental circular frequency ω_{1h}, which can be estimated by using Equation (4):

$$\lambda_{1h} = \frac{1}{\omega_{1h}^2} = \frac{T_{1h}^2}{4\pi^2} \tag{20}$$

Hence, the unknown parameters in the system of nonlinear equations in Equation (20) are the moments of inertia I_i. In other words, there are N unknown moments of inertias if the structure is a N-story frame. Equation (19) can be seen as a simple optimization problem. The roots of the nonlinear system of equations can be found by the function *fsolve*, which is a part of Matlab's *Optimization Toolbox* [15].

3.2 Structural parameters in the vertical direction

For vibration in the vertical direction the seismic mass is simply defined by the associated floor tributary area. From Figure 11b it can be seen that the seismic mass of the exterior column is equal to the half of the mass acting on the interior column:

$$m_{iv}^{(m)} = \frac{1}{2} m_v^{(story)} \tag{21}$$

$$m_{iv}^{(l)} = m_{iv}^{(r)} = \frac{1}{4} m_v^{(story)} \tag{22}$$

When the structure vibrates in its vertical fundamental mode (see Figure 11a) the vertical springs in Figure 9c represent the flexural stiffness of the girders. The POIs are assumed to be located at column mid-heights and beam mid-spans as shown in Figure 11a. The equivalent stiffness of the vertical springs c_{ui} can be obtained from Equation (23), which is analogous to Equation (17):

$$c_{ui} = \frac{3EA_iI_i\,(h + 12l)}{3I_ih^2 + A_ihl^3 + 36I_ihl + 3A_il^4} \tag{23}$$

The eigenvalue problem formulated in terms of the linear fundamental mode shape and the corresponding eigenvalue in the vertical direction leads to:

$$(\mathbf{M}_v - \lambda_{1v}\mathbf{K}_v)\,\boldsymbol{\phi}_1 = \mathbf{0} \tag{24}$$

The first eigenvalue in the vertical direction can be estimated by using Equation (5):

$$\lambda_{1v} = \frac{1}{\omega_{1v}^2} = \frac{T_{1v}^2}{4\pi^2} \tag{25}$$

The unknown variables are the cross sectional areas A_i, which can determined using simple optimization techniques.

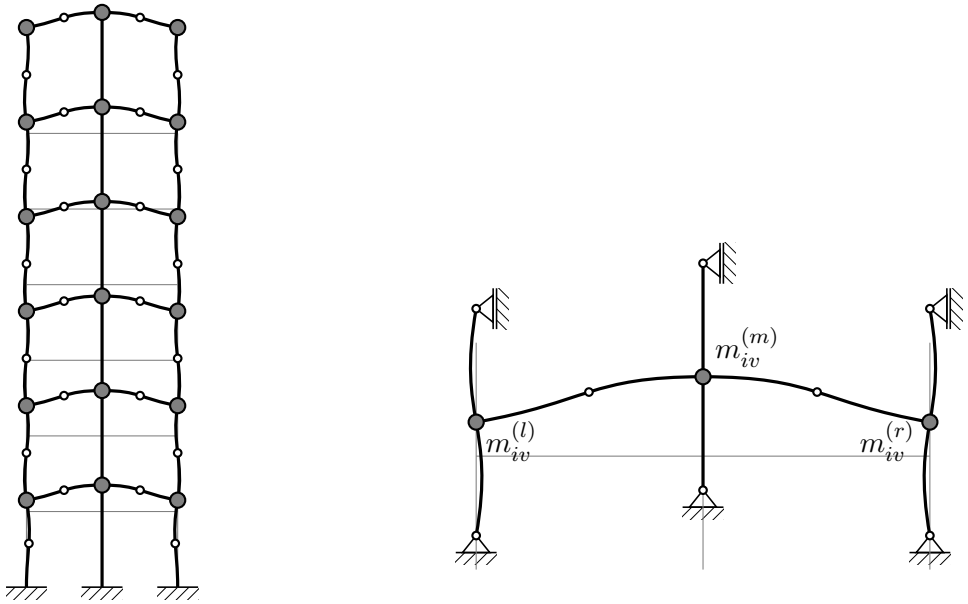

(a) (b)

Figure 11: Generic frame vibrating in its vertical linear fundamental mode. (a) Complete generic frame and (b) isolated substructure.

3.3 Evaluation of structural parameters

The parameters of the generic stick model are determined based on the mass and geometric characteristics outlined below.

- Seismic active story mass for vibration in the horizontal direction:

$$m_h^{(story)} = 229\,741\,\text{kg} \approx 230\,\text{t} \approx 10\,000\,\text{kip} \tag{26}$$

- Seismic active story mass for vibration in the vertical direction:

$$m_v^{(story)} = 19\,271\,\text{kg} \approx 19\,\text{t} \approx 830\,\text{kip} \tag{27}$$

- Story height, h, and bay width, l:

$$h/l = 1/2, \quad h = 3.96\,\text{m} = 13\,\text{ft} \tag{28}$$

Substituting Equation (28) into Equation (23) leads to a simplified formulation for the stiffness of the equivalent vertical springs:

$$c_{ui} = \frac{1}{\frac{7}{75}\frac{l^3}{EI_i} + \frac{1}{2}\frac{l}{EA_i}} \tag{29}$$

Equations (26) and (27) are substituted into Equations (15) and (21) to define the seismic mass in each story in the vertical and horizontal direction.

Performing the optimization problem defined by the eigenvalue problems in Equations (19) and (24) for generic stick models with $N = 3, 6, 12,$ and 24 stories leads to the moments of inertia I_i and the area A_i of the cross sections of the generic stick.

Figure 12a shows the ratio between the moment of inertia of the cross section in the ith floor I_i and the cross section of the first floor I_1. The same variation of this parameter over the structure's height is applied to all generic stick models with different number of stories. The moment of inertia decreases with an increase in height. This behavior is consistent with the variation of moment of inertia found in real perimeter steel moment-resisting frames [4, 19, 20]. In contrast, the profiles of the normalized area of the cross sectional area A_i/A_1 are shown in Figure 12b. The 3-, 6-, and 12-story structures have distributions of cross sectional area consistent with the corresponding profiles of the moments of inertia. However, for the 24-story generic steel model, the cross sectional area grows with increasing height up to approximately $2/3\, h_{rel}$, which is not consistent with the distribution of cross sectional areas in real perimeter frames. A reasonable explanation is that the generic structure is based on results (fundamental modes and corresponding periods) of real structures. A qualitative evaluation of the difference between the fundamental periods predicted from regression equations and their associated data points, as shown in Figures 8a and 8b, leads to the conclusion that the error is larger for tall structures than for low-rise structures. This is another reason why the profile of the relative cross sectional-areas of the 24-story generic stick model deviates from that of the actual structure.

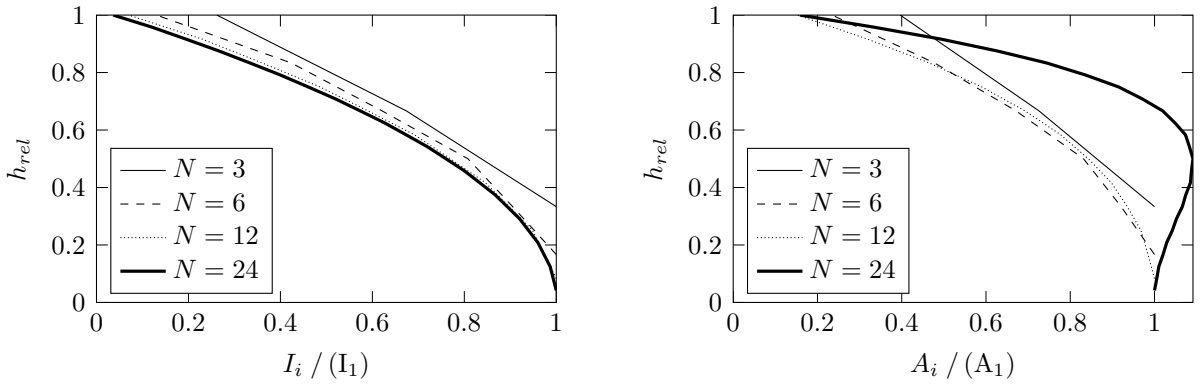

(a) (b)

Figure 12: Distribution of (a) the moments of inertia I_i and (b) the areas A_i of the cross sections over the relative height for the generic stick models used in this study.

4 RESULTS

4.1 Profiles of the vertical peak floor acceleration demand

Profiles of vertical peak floor acceleration demands PFA_v normalized to the vertical peak ground acceleration PGA_v due to ground motions of the VGM record set are shown in Figure 13. Gray lines show profiles of single records, bold black curves indicate statistical measures.

PFA_v demands increase with the number of stories (or vertical period). The maximum median amplification occurs for all structures at the roof level and it is approximately $4PGA_v$.

The importance of higher modes can be observed by evaluating the behavior of the 6-story frame (Figure 13b). In this case, the structure is tuned to a fundamental period in the vertical direction equal to $T_{1v} = 0.15\,\text{s} = 20/3\,\text{Hz}$. This period lies exactly on the lower corner frequency of the NEHRP-spectrum in Figure 1. Thus, the first few higher modes of the 6-story structure experience relatively high modal spectral acceleration demands, which causes an increase in

accelerations with respect to the 3-story structure. This behavior is also observed for the 12- and 20-story generic stick models.

These results show that, in general, PFA_v demands tend to vary linearly over the structure's height. The taller the structure, the more S-shaped the PFA_v profiles are. This behavior is also reported in a study of R.S. Chaudhuri [23] on the evaluation of PFA_h demands. While regression equations are proposed for the S-shaped PFA_h demand in [23], a very simple linear fitting equation could lead to a useful approximation of the PFA_v demands over the height of the structure.

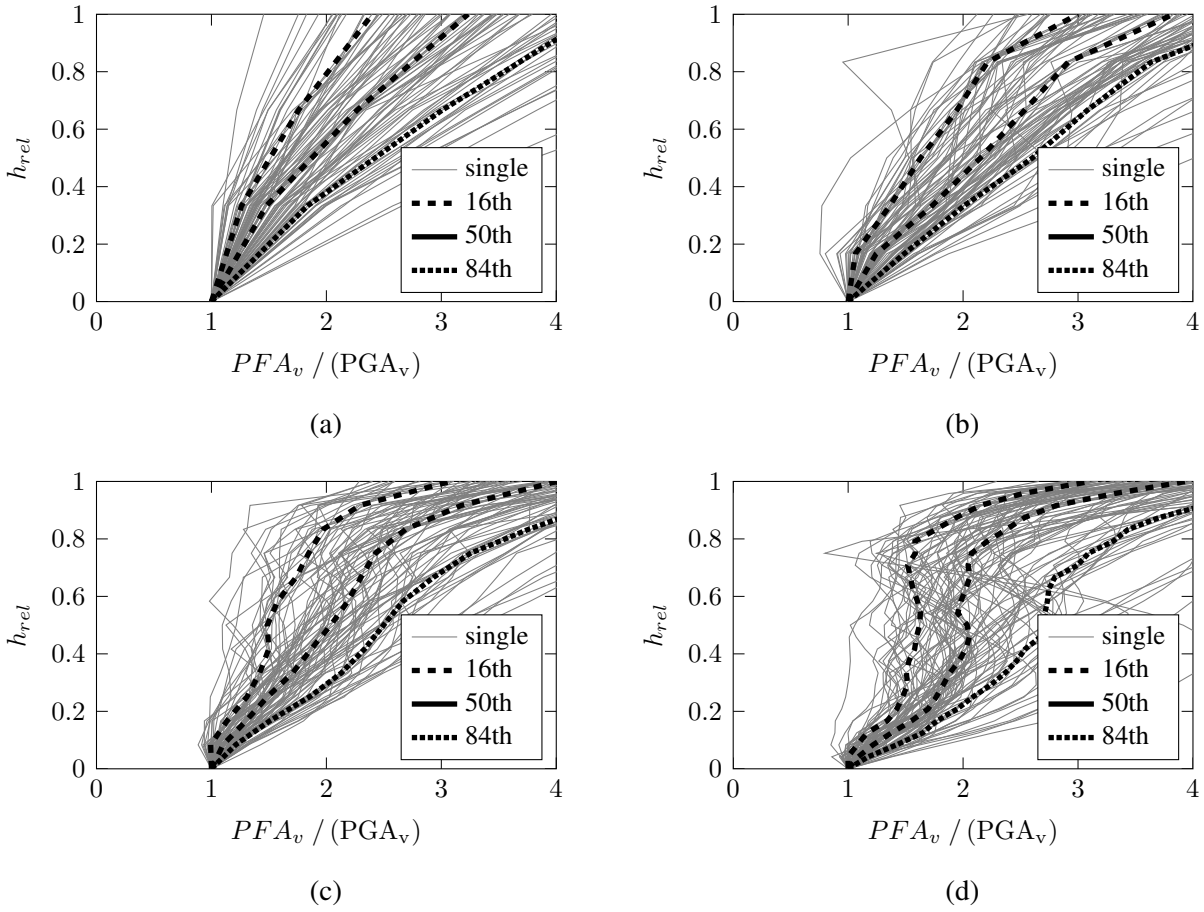

Figure 13: Profiles of the vertical peak floor acceleration demand normalized to the vertical peak ground acceleration for the (a) 3-story, (b) 6-story, (c) 12-story, and (d) 24-story generic stick models exposed to records from the VGM record set.

In order to evaluate the adequacy of Equation (1), which was developed for NSCs [1], Figure 14 shows the ratio of PFA_v to PGA_h. The vertical dash-dotted line at ${}^{PGA_v}/_{PGA_h} = {}^1/_2$ represents Equation (1) in terms of the vertical acceleration demand of a nonstructural component based on seismic design provision in the United States of America. It is evident from Figure 14 that the codified procedure leads to an underestimation of the PFA_v demand in contrast to the median profiles. As already mentioned, a linear variation of PFA_v over the height is a more representative characterization. A reasonable distribution analogous to the PFA_h (i.e. height factor) demand determined from the seismic equivalent lateral forces acting on NSCs defined in [1] would lead to a better approximation based on the results from this study.

At the base of the structures, the resulting PFA_v to PGA_h ratios are consistent with the V/H ratios discussed in the study of Bozorgnia and Campbell [7]. Traditionally, the $^{PGA_v}/_{PGA_h}$ ratio is assumed to be $^2/_3$, which is adequate for a median ratio. However, the 84th percentile value is larger than unity and the peak value is larger than two. Therefore, if the objective is to propose a codified procedure to estimate V/H ratios, a value greater than $^2/_3$ may be warranted.

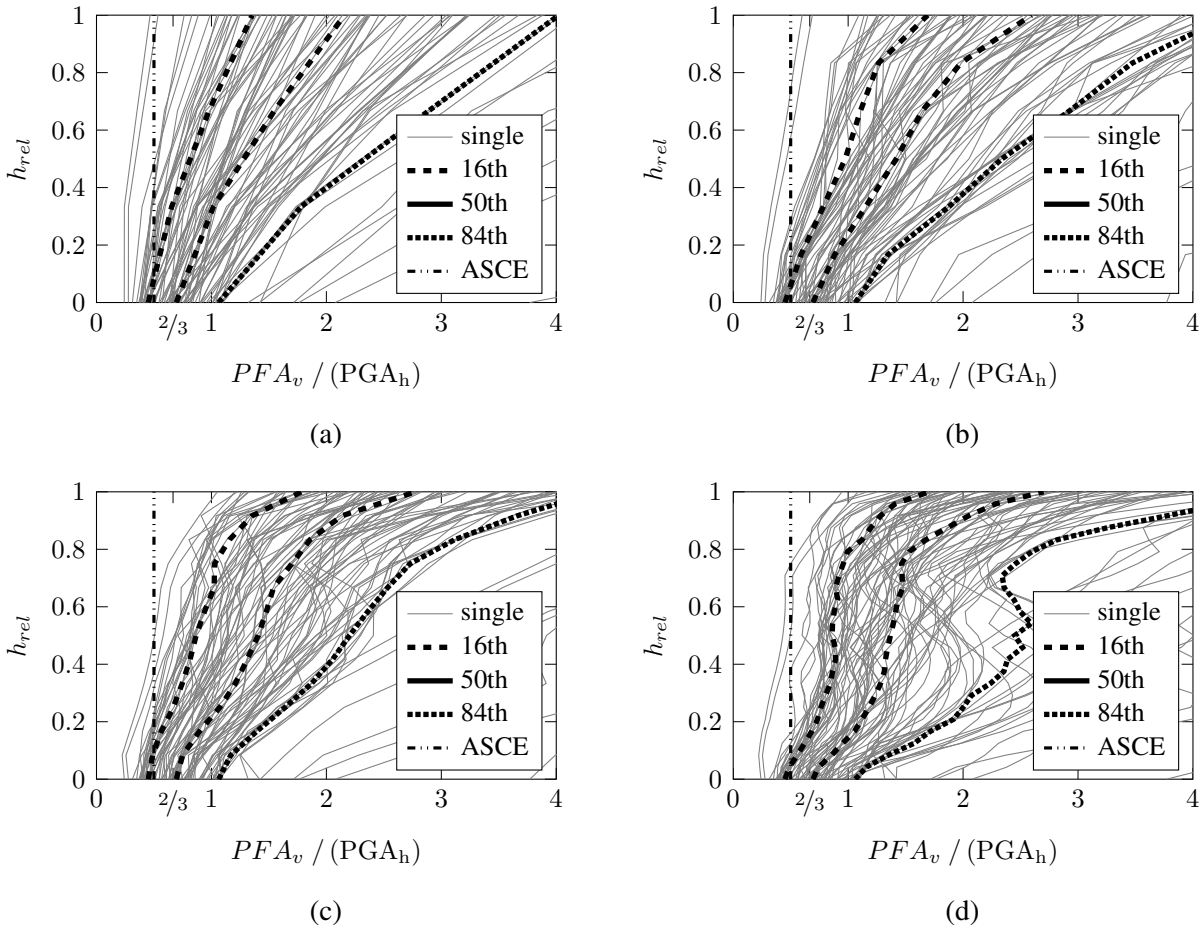

Figure 14: Profiles of the vertical peak floor acceleration demand normalized to the horizontal peak ground acceleration for the (a) 3-story, (b) 6-story, (c) 12-story and (d) 24-story generic stick models exposed to records from the VGM record set.

5 SUMMARY AND CONCLUSION

The focus of this paper is on the evaluation of vertical peak floor acceleration demands in elastic, regular perimeter frames of steel structures designed according to older [24] and more modern generations of U.S. design codes [25]. Rigorous treatment of the vertical peak floor acceleration (PFA_v) demand on NSCs is neglected in building codes since typical civil engineering buildings are assumed to behave rigidly in vertical direction.

This study highlights critical research needs as well as the importance of studying PFA_v demands for NSCs. The most salient observation from the results of this study is that neglecting the vertical component of the base acceleration may lead to a drastic underestimation of the vertical design forces for NSCs. This underestimation may lead to risk of injuries; loss of

functionality; and/or significant repair costs associated with damages to components, their supports, and attachments.

In this paper, a ground motion record set compatible with the recommended vertical design response spectrum in the United States of America [8] (in this report referred as NEHRP-spectrum) is generated and generic stick models of column lines in steel perimeter frames are designed. These generic structures were used to evaluate PFA_v demands close to the locations of columns in the structure.

The results from this study show that the vertical floor acceleration demands are in general much larger (up to a factor of three in the median) than the peak vertical ground acceleration. In addition, peak vertical floor accelerations tend to increase with height. These two observations are not explicitly accounted for in current design provisions in the United States of America, which may lead in many cases to the underestimation of vertical component design forces. However, these conclusions are based on assumptions made on numerical models and ground motion properties consistent with the ones used in this study. In addition, only record-to-record variability was accounted for.

REFERENCES

[1] American Society of Civil Engineers, *ASCE 7-10 - Minimum Design Loads for Buildings and Other Structures*, 2010.

[2] International Code Council, *IBC - International Building Code*, 2012.

[3] European Committee for Standardization, *EN 1998-1 - Design of Structures for Earthquake Resistance - Part 1: General Rules, Seismic Actions and Rules for Buildings*, 2013.

[4] J.D. Wieser, G. Pekcan, A.E. Zaghi, A.M. Itani, E. Maragakis, "Assessment of Floor Accelerations in Yielding Buildings", *MCEER reports*, ed. by University at Buffalo, State University of New York. Vol. 12-0008.

[5] ICC - Evaluation Service Inc., *AC156 - Acceptance Criteria for Seismic Qualification by Shake-Table Testing of Nonstructural Components and Systems*, 2007.

[6] K.W. Campbell, Y. Bozorgnia, Updated Near-Source Ground-Motion (Attenuation) Relations for the Horizontal and Vertical Components of Peak Ground Acceleration and Acceleration Response Spectra. *Bulletin of the Seismological Society of America*, **93**, 314–331, 2003.

[7] Y. Bozorgnia, K.W. Campbell, The Vertical-to-Horizontal Response Spectral Ratio and Tentative Procedures for Developing Simplified V/H and Vertical Design Spectra. *Journal of Earthquake Engineering*, **8**, 175–207, 2004.

[8] Applied Technology Council, *FEMA P-750 - NEHRP Recommended Seismic Provisions for New Buildings and Other Structures*, 2009.

[9] USGS, *Geologic Hazards Science Center - U.S. Seismic Design Maps*, 2010.

[10] K.W. Campbell, Y. Bozorgnia, NGA Ground Motion Model for the Geometric Mean Horizontal Component of PGA, PGV, PGD and 5% Damped Linear Elastic Response Spectra for Periods Ranging from 0.01 to 10 s. *Earthquake Spectra*, **24**, 139–171, 2008.

[11] A.E. Seifried, "Response Spectrum Compatibilization and its Impact on Structural Reponse Assessment", PhD thesis, Stanford CA: Stanford University, 2013.

[12] Pacific Earthquake Engineering Research Center, *PEER - Ground Motion Database*, 2010.

[13] W.B. Joyner, D.M. Boore, Peak Horizontal Acceleration and Velocity from Strong-Motion Records Including Records from the 1979 Imperial Valley, California, Earthquake. *Bulletin of the Seismological Society of America*, **71**, 2011–2038, 1981.

[14] K.W. Campbell, Y. Bozorgnia, "Engineering Characterization of Ground Motion", *Earthquake Engineering*, ed. by Y. Bozorgnia, V.V. Bertero. CRC Press, 2004.
[15] The MathWorks Inc., *MATLAB - Global Optimization Toolbox*, 2013.
[16] N. Shome, "Probabilistic Seismic Demand Analysis of Nonlinear Structures", PhD thesis, Stanford, CA: Stanford University, 1999.
[17] National Institute of Standards and Technology, *NIST GCR 11-917-15 - Selecting and Scaling Earthquake Ground Motions for Performing Response-History Analysis*, 2011.
[18] A. Abraham, L.C. Jain, R. Goldberg. *Evolutionary Multiobjective Optimization: Theoretical Advances and Applications*. Springer, 2005.
[19] A. Gupta, "Seismic Demands for Performance Evaluation of Steel Moment Resisting Frame Structures", PhD thesis, Stanford CA: Stanford University, 1999.
[20] National Institute of Standards and Technology, *NIST GCR 10-917-8 - Evaluation of the FEMA P-695 Methodology for Quantification of Building Seismic Performance Factors*, 2010.
[21] L. Moschen, R.A. Medina, C. Adam, *Final Report for the Marshall Plan Scholarship - Vertical Acceleration Demands on Nonstructural Components in Buildings*, 2014.
[22] R.A. Medina, "Seismic Demands for Nondeteriorating Frame Structures and Their Dependence on Ground Motions", PhD thesis, Stanford CA: Stanford University, 2003.
[23] R.S. Chaudhuri, T.C. Hutchinson. Distribution of Peak Horizontal Floor Acceleration for Estimating Nonstructural Element Vulnerability. *Proceedings of the 13th World Conference on Earthquake Engineering (13WCEE)*, Vancouver, British Columbia, Canada, Paper No. 1721, August 1-6, 2004.
[24] International Conference of Building Officials, *UBC - Uniform Building Code Vol. 2 - Structural Engineering Design Provisions*, 1994.
[25] International Code Council, *IBC - International Building Code*, 2009.